

Degradation of 2.4-kV Ga₂O₃ Schottky Barrier Diode at High Temperatures up to 500 °C

Hunter Ellis, Wei Jia, Imteaz Rahaman, Apostoli Hillas, Botong Li, Michael A. Scarpulla, Berardi Sensale Rodriguez, Kai Fu

Abstract— Ga₂O₃ Schottky barrier diodes featuring a field plate and a composite SiO₂/SiN_x dielectric layer beneath the field plate were fabricated, achieving a breakdown voltage of 2.4 kV at room temperature. Electrical performance and degradation were analyzed via *I-V* and *C-V* measurements from 25 °C to 500 °C, revealing temperature-dependent transport, interface stability, and device stability. Upon returning to room temperature, the diodes exhibited nearly unchanged forward characteristics, while the breakdown voltage declined significantly from 2.4 kV to 700 V. This behavior indicates a temperature-induced reduction in the barrier height. Detailed analysis revealed that variable range hopping (VRH) dominated the leakage mechanism at moderate temperatures, while thermal emission (TE) became increasingly significant at temperatures exceeding 400 °C.

Index Terms— β -Ga₂O₃, Extreme Environment, Schottky Barrier Diode, High-Voltage

I. INTRODUCTION

POWER electronics play a critical role in minimizing system power loss, but they encounter challenges in high-temperature environments such as deep oil drilling, planetary exploration, turbine engines, and geothermal energy systems [1], [2], [3], [4]. Wide bandgap and ultra-wide bandgap semiconductors present promising solutions to these challenges. Among them, β -Ga₂O₃ stands out due to its exceptional properties, including a wide bandgap of 4.85 eV, a high breakdown electric field of 8 MV/cm, and a melting point of 1800 °C [5]. Additionally, β -Ga₂O₃'s low intrinsic carrier density of $1.79 \times 10^{-23} \text{ cm}^{-3}$ ensures that the intrinsic carrier concentration remains significantly lower than the doping levels, even at elevated temperatures [6]. These characteristics make β -Ga₂O₃ an excellent candidate for high-temperature applications [7], [8].

Schottky barrier diodes (SBD) are one of the fundamental and crucial power devices [9], [10], [11]. β -Ga₂O₃-based SBDs have been extensively studied by numerous research groups [12], [13], [14], [15], [16]. Recently, it has been observed that the Schottky contacts on β -Ga₂O₃ experience significant degradation in both forward and reverse performance at elevated temperatures [17], [18], [19], [20], [21]. For example,

This work is supported in part by the University of Utah start-up fund and PIVOT Energy Accelerator Grant U-7352FuEnergyAccelerator2023. (Corresponding author: Kai Fu). Hunter Ellis and Wei Jia contributed equally, or if there are co-first authors.

The authors are with the Electrical and Computer Engineering Department, the John and Marcia Price College of Engineering, the University of Utah, Salt Lake City, UT 84112, USA.

Ga₂O₃ SBDs have severely reduced breakdown voltages (BV) and increased leakage current at temperatures from 300 °C to 500 °C, with the leakage current rising by a factor of 10⁴ and the BV decreasing by more than ten times compared to room temperature (RT) [19], [20]. Despite its significance, this issue remains unexplored and insufficiently analyzed.

In this work, β -Ga₂O₃ Schottky barrier diodes are fabricated with a breakdown voltage of 2.4 kV at room temperature, and their degradation is investigated at high temperatures up to 500 °C. Key parameters such as ideality factor, barrier height, interface state density, leakage current, and breakdown voltage are analyzed through both *I-V* and *C-V* measurements. The underlying leakage mechanisms are also examined through detailed characterization.

II. DEVICE FABRICATION AND MEASUREMENTS

The β -Ga₂O₃ diode structure was fabricated using a β -Ga₂O₃ wafer sourced from Novel Crystal Technology, Inc. The wafer featured a 10 μm thick drift layer with a doping concentration of $1 \times 10^{16} \text{ cm}^{-3}$, grown on a (001) Sn doped n⁺- β -Ga₂O₃ substrate. The fabrication process is shown in Fig. 1(a). A 35 μm thick photoresist was employed for etching β -Ga₂O₃, resulting in a 1 μm deep trench isolation and lifting off the following dielectric. The dielectric layer was deposited by alternating the sputtering of 40 nm layers of SiO₂ and SiN_x, repeated until the 1 μm deep trench was fully filled. Subsequently, Pt (50 nm)/Au (250 nm) alloy was deposited to form a Schottky contact on the β -Ga₂O₃ and a field plate (FP) on the dielectric simultaneously. The diode has a diameter of 200 μm , with a FP length of 45 μm . Finally, Ti (50 nm)/Au (250 nm) was deposited on the bottom surface to form the ohmic

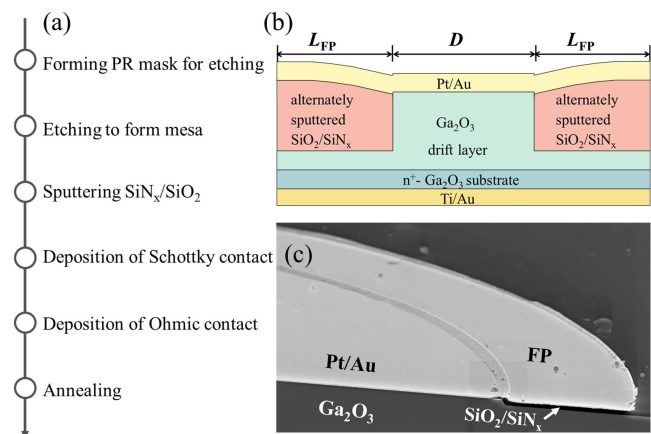


Fig. 1. (a) Process flow. (b) Schematic of the β -Ga₂O₃ SBD structure. (c) SEM image showing the cross-section of the SBD.

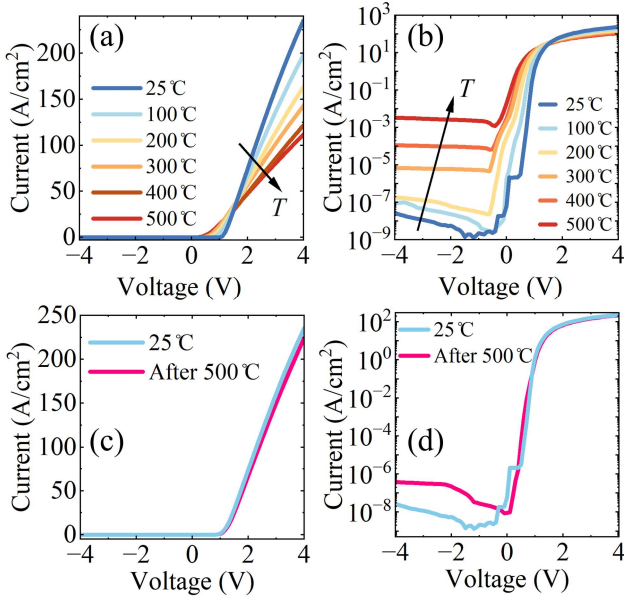


Fig. 2. (a) Linear and (b) semi-log forward I - V curves from 25 °C to 500 °C. Comparison of I - V curves before and after 500 °C in (c) linear and (d) semi-log scale.

contact. An SEM image of the device structure is shown in Fig. 1(b). The forward I - V and C - V measurements were characterized using a 4200A-SCS parameter analyzer, while the breakdown voltage was measured up to 1000 V using a Keithley 2470 SourceMeter. For higher voltages, up to 10 kV, a Matsusada AU30N5 was used, with 3M™ Fluorinert™ Electronic Liquid FC-40 applied to prevent air breakdown.

III. FORWARD PERFORMANCE AT HIGH TEMPERATURES

Figure 2(a) and (b) present the forward I - V curves of the β - Ga_2O_3 diode in linear and semi-log scales, respectively, measured from 25 °C to 500 °C. The reverse leakage current increased significantly with temperature (from 10^{-8} to 10^{-3} A/cm²), while the on-current declined. The devices were held at each temperature for 1 hour. Figure 2(c) and (d) illustrate the recovery behavior of the diode after testing up to 500 °C. After 5 hours of high-temperature storage, the forward current fully recovered, but the reverse leakage current exhibited a minor and permanent increase from 10^{-8} to 10^{-7} A/cm².

Figure 3(a) presents the ideality factor, which increases with temperature, likely due to a nonhomogeneous Schottky contact with temperature-dependent interface state densities [22], [23], [24], [25], [26]. Figure 3(b) shows the rectifying ratio at ± 4 V, which decreases with temperature as the off-current increases and the on-current decreases. The turn-on voltage (defined at 100 μ A) also decreases with rising temperature, primarily due to increased leakage current. Figure 3(c) and (d) depict the temperature-dependent equivalent series (R_s) and parallel resistance (R_p), respectively. The R_s increases with temperature due to reduced mobility at higher temperatures [19] since the carrier concentration does not change much with the temperature (Fig. 4(b)), while R_p decreases, likely driven by faster trap de-trapping rates and elevated thermal emission currents [27].

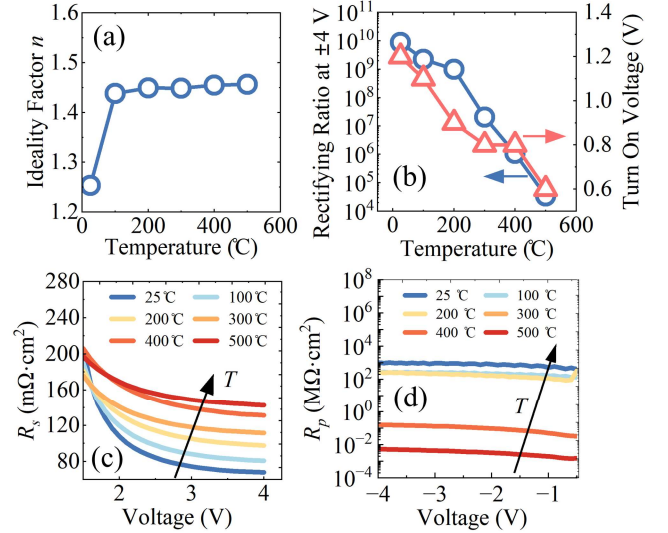


Fig. 3. (a) Ideality factor of the Ga_2O_3 diode at different temperatures. (b) Rectifying ratio at ± 4 V and the turn-on voltage from 25 °C to 500 °C. (c) Derived series (R_s) and (d) parallel (R_p) resistance as a function of temperature.

Figure 4(a) displays the C - V measurements at 1 MHz, while Fig. 4(b) illustrates the ionized donor's depth profile from 25 °C to 500 °C, with an average doping concentration of 1×10^{16} cm⁻³ calculated from the C - V data. Figure 4(c) presents the C^{-2} - V plots across the same temperature range, with the inset depicting a equivalent circuit model of the diode's capacitance [28]. This model incorporates the depletion capacitance beneath the Schottky contact (C_D), in parallel with the FP capacitance from the dielectric (C_{FP}) and the depletion capacitance beneath the FP in the β - Ga_2O_3 (C_{FD}), describing the total system capacitance as given by Eq. (1).

$$C = C_d + (C_{FP} \times C_{FD} / (C_{FP} + C_{FD})) \quad (1)$$

$$C = C_d + C_{FP} \quad (2)$$

$$C = b_1(V - \phi_{bi})^{-1/2} + b_2 \quad (3)$$

$$C_D = (q\epsilon_s N_D / 2(V - \phi_{bi}))^{1/2} \quad (4)$$

Given that C_{FP} is significantly smaller than C_{FD} due to the dielectric's thickness of 1 μ m, Eq. (1) can be approximated by Eq. (2). The data was subsequently fitted by minimizing the mean squared error in Eq. (3) for b_1 and b_2 . Here, b_1 represents the coefficient for the voltage-dependent capacitance C_D , b_2 corresponds to C_{FP} , V denotes the applied voltage, and ϕ_{bi} is the built-in potential [28]. The equation for C_D is given in Eq. (4), where N_D is the donor concentration, q is the charge of an electron, and ϵ_s is the permittivity of β - Ga_2O_3 . With the increase of reverse bias, the C^{-2} data deviates from linearity due to the influence of the additional FP capacitance [29]. Fig. 4(d) shows a magnified view of C^{-2} - V data from Fig. 4(c), revealing an increase in capacitance with temperature. The trend suggests a reduction in depletion width, which can be attributed to a decrease in barrier height.

To examine the barrier height variation, it was derived from both I - V and C - V measurements for comparison. The saturation current I_0 , a key parameter for determining the barrier height from the I - V curve, was obtained from the intercept of the

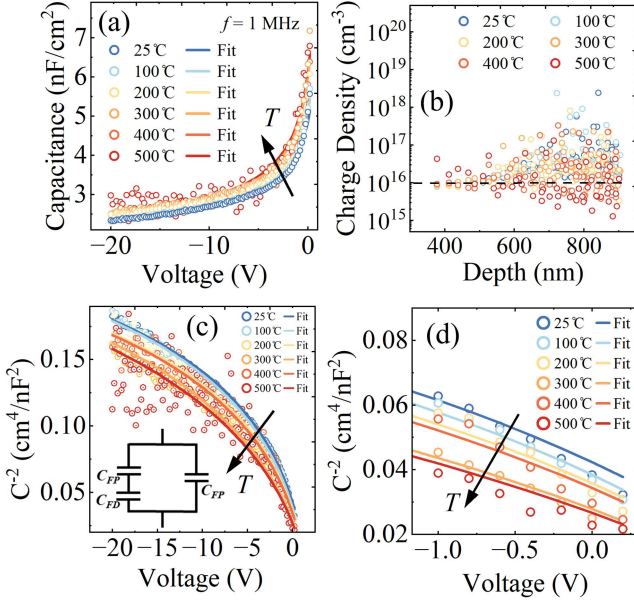


Fig. 4. (a) C - V curves from 25 °C to 500 °C. (b) Charge density in the Ga₂O₃. (c) C^{-2} - V curves at different temperatures, with inset showing the equivalent circuit considering the capacitance under the field plate (FP). (d) C^{-2} - V at different temperatures showing the shift of built-in potential.

extrapolated I - V data, as shown in Fig. 5(a). The derived I_0 values across the temperature range from room temperature to 500 °C are presented in Fig. 5(b). Based on the expression for I_0 given in Eq. (5), I_0 increases with temperature, where A^* is the Richardson constant for β -Ga₂O₃ (41 A·cm⁻²·k⁻²) [30], k is the Boltzmann constant, ϕ_b is the barrier height, A is the area of the diode, and T is the temperature. Interestingly, we observed that I_0 increases linearly with the temperature (in °C) on log-log scale. The empirical relationship is expressed in Eq. (6).

$$I_0 = AA^*kT^2 \exp(q\phi_b/kT) \quad (5)$$

$$\log(I_0) = 9.63 \times \log(T) - 31.53 \quad (6)$$

Figure 5(c) compares the barrier height (ϕ_b) and the built-in potential (ϕ_{bi}) derived from I - V and C - V measurements, where their relationship is described in Eq. (7), with N_c representing the effective density of states of conduction band [29]. The observed discrepancy between ϕ_b and ϕ_{bi} values from I - V and C - V methods suggests an inhomogeneous Schottky barrier [22], [30], usually caused by interface defects, metal grain boundaries, and/or contact non-uniformities [31], [32]. A simplified model, illustrated in Fig. 5(d), represents the diode as having two distinct barrier heights and corresponding I_0 . This diode can be extended to a simplified model, as shown in Fig 5(d), to represent a diode with two distinct barrier heights. This model can be extended to include multiple parallel diodes or a continuous distribution of barrier heights, capturing the complexity of real-world barrier inhomogeneities [22], [28], [33], [34], [35], [36], [37].

$$\phi_b = \phi_{bi} + kT \ln(N_c/N_D) \quad (7)$$

The barrier height calculated from I - V measurements is primarily influenced by the regions with lower barrier heights, as it is derived from I_0 , which is exponentially sensitive to ϕ_b .

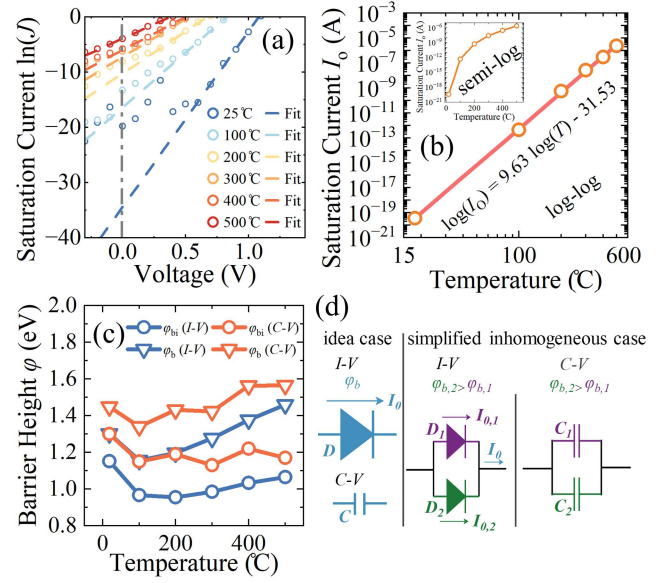


Fig. 5. (a) linear fitting for forward I - V data. (b) I_0 from 25 °C to 500 °C. (c) Schottky barrier height ϕ_b and built-in potential ϕ_{bi} as a function of temperature derived from the I - V and C - V curves. (d) Schematics of ideal Schottky diode with leakage current I_0 , simplified inhomogeneous Schottky diode with two distinct barriers represented by D_1 and D_2 , and equivalent capacitive circuits.

In the simplified case of two distinct barriers, as depicted in Fig. 5(d), the total I_0 is given by Eq. (8), where $I_{0,1}$ and $I_{0,2}$ represent the saturation currents for diodes D_1 and D_2 , respectively. Given the exponential dependence of I_0 on ϕ_b as shown in Eq. (5), even minor variations in ϕ_b can lead to significant changes in I_0 , highlighting the dominance of lower barriers in determining the I - V -derived barrier height.

$$I_0 = I_{0,1} + I_{0,2} \quad (8)$$

For example, let $\phi_{b,1}$, the barrier height for D_1 , be 1 eV, and $\phi_{b,2}$, the barrier height for D_2 , be 1.15 eV. These values result in $I_{0,1} = 5.1 \times 10^{-15}$ A/cm² and $I_{0,2} = 1.6 \times 10^{-17}$ A/cm². Since $I_{0,1}$ is nearly two orders of magnitude larger than $I_{0,2}$, Equation (7) can be approximated by considering only $I_{0,1}$.

In contrast, the barrier heights obtained from C - V measurements reflect the combined capacitance contributions of both diodes, as modeled in the parallel capacitor circuit in Fig. 5(d). The total capacitance C_{tot} , calculated using Eq. (9), is the area-weighted sum of the individual capacitances (C_1 and C_2), where A_1 and A_2 are the respective contact areas.

$$C_{tot} = (A_1 C_1 + A_2 C_2) / A \quad (9)$$

As defined in Eq. (r), the capacitance of an SBD has a square-root dependence on ϕ_{bi} , such that small variations in ϕ_{bi} lead to only minor changes in the capacitance. For the barrier heights considered in the previous example, the corresponding capacitances are $C_1 = 28$ nF and $C_2 = 26$ nF based on the ϕ_{bi} . The relatively small difference between C_1 and C_2 suggests that barrier heights derived from C - V measurements are less sensitive to lower barrier regions in inhomogeneous systems compared to those obtained from I - V measurements.

IV. INTERFACE DENSITY

Figure 6(a) displays the room-temperature C - V data measured across frequencies from 1 MHz to 7 kHz, highlighting the frequency-dependent behavior of interface states in the SBD. At frequencies above 100 kHz, the interface states have time constants too large to contribute significantly, resulting in minimal capacitance variation between 100 kHz and 1 MHz. In contrast, at lower frequencies, such as 7 kHz, all interface states can respond, causing the capacitance to stabilize at the same value observed at 10 kHz. Figure 6(b) depicts the interface state density (N_{ss}), which increases with temperature, correlating with the observed rise in leakage current. N_{ss} is calculated using Eq. (10), where $C_{LF}(V)$ and $C_{HF}(V)$ represent the low-frequency (7 kHz) and high-frequency (1 MHz) capacitances, respectively [38], [39].

$$N_{ss} = (q\epsilon_s N_D / 2\phi_{bi})^{1/2} \times (C_{LF}(V) - C_{HF}(V)) \times q C_{HF}(V) \quad (10)$$

The energy level of the interface state (E_{ss}) was calculated using Eq. (11), where E_c is the conduction band energy, and ϕ_e is the effective barrier height. ϕ_e is defined in Eq. (12) and derived from barrier height ($\phi_{b,iv}$) obtained from I - V measurements [40].

$$E_c - E_{ss} = q(\phi_e - V) \quad (11)$$

$$\phi_e = \phi_{b,iv} + (1 - n^{-1})V \quad (12)$$

Figure 6(c) illustrates a band diagram representing N_{ss} , which also highlights ϕ_o , the neutral level, which serves as the boundary: interface states above ϕ_o exhibit acceptor-like behavior, while those below ϕ_o exhibit donor-like behavior.

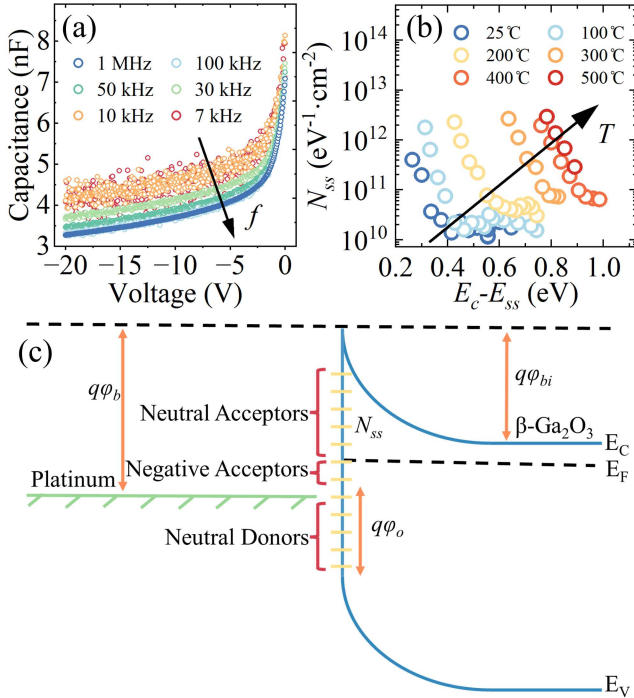


Fig. 6. (a) C - V curves from 1 MHz to 7 kHz. (b) Interface state density at the interface of the Schottky contact and the β - Ga_2O_3 from 25 °C to 500 °C. (c) Schematic of energy band diagram showing interface states.

V. REVERSE PERFORMANCE AT HIGH TEMPERATURES

Figure 7(a) shows the reverse bias I - V curve at 25 °C with a breakdown voltage of around 2.4 kV, corresponding to an electric field strength of around 3.3 MV/cm. The inset displays a cleaved device post-breakdown. Figure 7(b) depicts reverse bias I - V curves from 25 °C to 500 °C, revealing a significant increase in leakage current with temperature, particularly beyond 200 °C. The breakdown voltage, initially above 1 kV at 25 °C and 100 °C, dropped to 700 V at 200 °C and fell below 100 V at higher temperatures. Figure 7(c) compares the reverse I - V characteristics before and after 500 °C testing, revealing a permanent reduction in breakdown voltage to 650 V. The degradation is expected to be attributed to increased interface states, reduced barrier height, and/or potential contact diffusion into the diode during high-temperature exposure [18], [41].

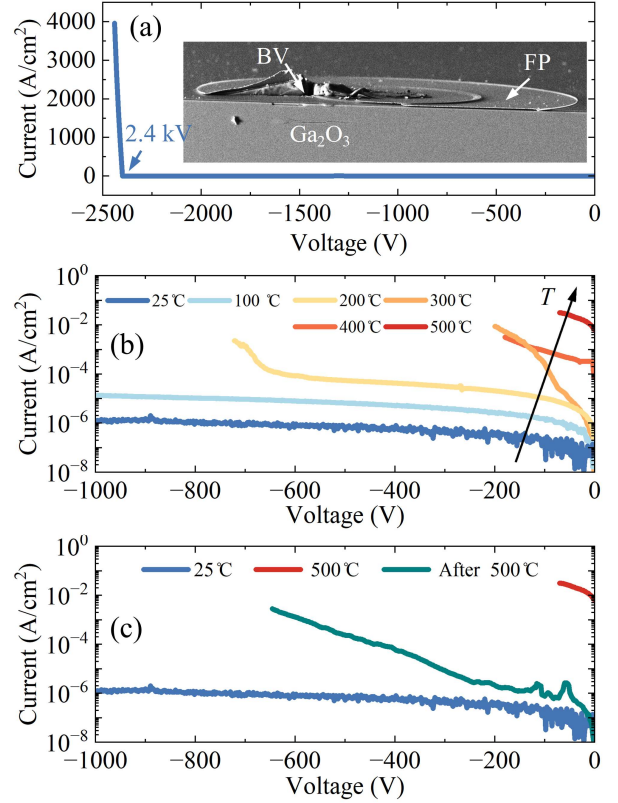


Fig. 7. (a) Reverse breakdown I - V curve of the Ga_2O_3 SBD at room temperature. The inset shows the cross-section of a diode after breakdown. (b) Reverse I - V curves of the β - Ga_2O_3 SBD from 25 °C to 500 °C. (c) Comparison of the reverse I - V curves of the Ga_2O_3 SBD at 25 °C, at 500 °C, and after 500 °C.

Analysis of the reverse I - V data reveals that leakage current scales linearly with area, as shown in Fig. 8(a), indicating that surface leakage is negligible. From 25 °C to 200 °C, the leakage mechanism follows the variable range hopping (VRH) model. Fitting results for the VRH process are presented in Fig. 8(b) and 8(c) for voltage ranges of 24–62 V and 100–700 V, respectively. The VRH current density (J_{VRH}) was calculated using Eq. (6), where T_c is the characteristic temperature [42], [43].

$$J_{VRH} \propto \exp(- (T_c/T)^{1/4}) \quad (13)$$

With the increase of temperature, the leakage due to thermal emission (TE) becomes significant. Both TE and VRH account

for the leakage. Figure 8(d) shows the VRH fitting for the data taken from 300 °C to 500 °C with the TE current subtracted. We have found that the T_c in the VRH model increases with temperature under reverse bias, suggesting changes in material disorder or carrier transport dynamics. This could be attributed to: (a) activation of deeper trap states at higher temperatures, increasing the effective density of localized states and broadening energy levels involved in hopping; (b) enhanced carrier localization due to thermally activated occupancy of more localized states under reverse bias, reducing hopping distances. Figure 8(e) compares the measured current density with the simulated TE, VRH, and the combined contributions. TE modeled using Eq. (14), where J_{TE} is TE the current density [22], and E is the electric field at metal- β -Ga₂O₃ interface [44]. Figure 8(f) illustrates the calculated TE leakage current at 500 °C for a β -Ga₂O₃ diode with varying barrier heights. The results show that a high barrier height (e.g., > 2 eV), is crucial for suppressing current leakage at elevated temperatures.

$$J_{TE} \propto A^* T^2 \exp(-q\phi_{b,iv} - (qE/4\pi\epsilon_s)^{1/2})(kT)^{-1} V_o \quad (14)$$

$$V_o = (\exp(-qV/kT)) - 1 \quad (15)$$

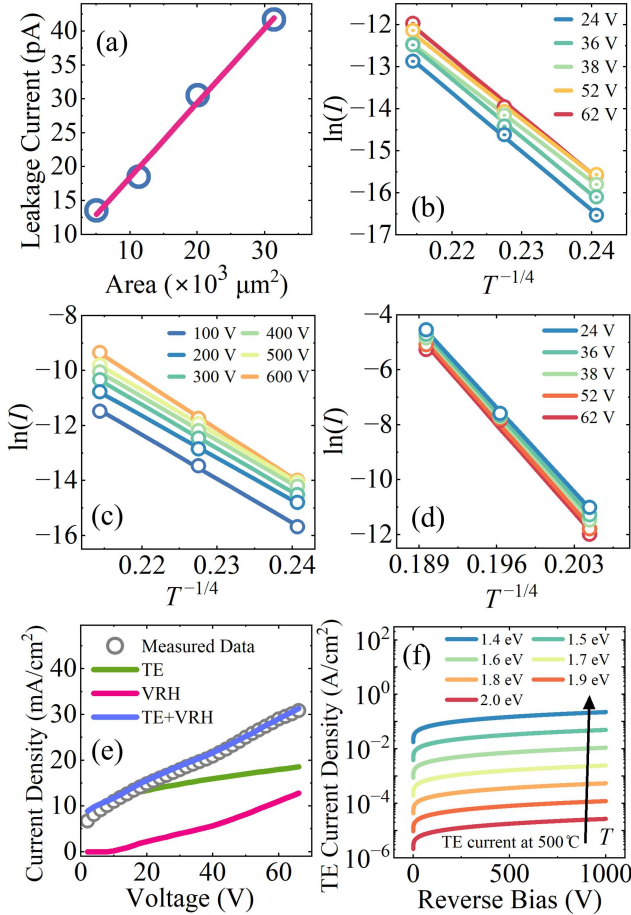


Fig. 8. (a) Leakage current vs device contact area. Fitting curves based on VRH transportation at (b) low-temperature and low-voltage, (c) low-temperature and high-voltage, and (d) high-temperature and low-voltage. (e) Comparison of measured leakage current and calculated leakage current based on TE and VRH transport models. (f) Simulated reverse I - V with the barrier height varying from 1.4 eV to 2.0 eV.

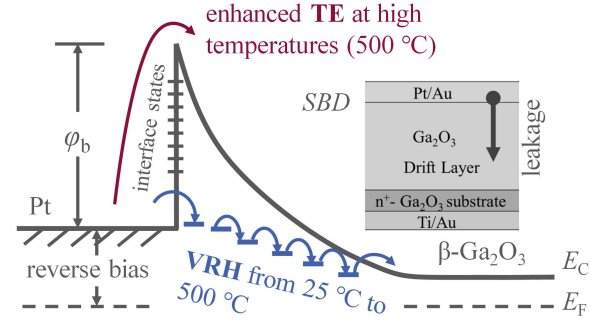


Fig. 9. Schematic of leakage mechanisms at high temperatures.

Figure 9 presents the band diagram of a β -Ga₂O₃ SBD to indicate the dominant leakage mechanisms across different temperatures. The VRH model prevails at intermediate temperatures, while the TE becomes increasingly significant as the temperature approaches 500°C.

VI. CONCLUSION

A β -Ga₂O₃ SBD with a breakdown voltage of 2.4 kV was fabricated and analyzed via I - V and C - V measurements over 25°C to 500°C. Results revealed an inhomogeneous Schottky interface with increasing interface state densities and discrepancies between C - V and I - V barrier heights, contributing to elevated leakage currents and reduced breakdown voltage at higher temperatures. The dominant leakage mechanism transitioned from VRH to TE above 400°C. After cooling, the device retained forward characteristics, but the breakdown voltage decreased to 700 V.

Improving high-temperature performance could involve optimizing surface treatments, contact metallurgy, and employing metals with higher, stable work functions to mitigate TE leakage. Alternative designs, such as Schottky diodes made with PbCoO₂ and platinum group metal oxide contacts, have demonstrated resilience to high temperatures with low reverse and forward biases [10], [17], [45], [46]. Besides, devices employing pn heterojunctions, like NiO/ β -Ga₂O₃ diodes, have shown improved performance, maintaining breakdown voltages above 1 kV even at high temperatures [20], [47], [48], [49], attributed to higher built-in voltages, larger depletion regions, and reduced defect densities [28].

ACKNOWLEDGMENT

The device fabrication was performed at the Nanofab at the University of Utah.

REFERENCES

- [1] J. Watson and G. Castro, "A review of high-temperature electronics technology and applications," *J. Mater. Sci. Mater. Electron.*, vol. 26, pp. 9226–9235, 2015.
- [2] P. G. Neudeck, R. S. Okojie, and L.-Y. Chen, "High-temperature electronics—a role for wide bandgap semiconductors?," *Proc. IEEE*, vol. 90, no. 6, pp. 1065–1076, 2002.
- [3] P. G. Neudeck *et al.*, "Operational testing of 4H-SiC JFET ICs for 60 days directly exposed to Venus surface atmospheric

- conditions,” *IEEE J. Electron Devices Soc.*, vol. 7, pp. 100–110, 2018.
- [4] R. W. Johnson, J. L. Evans, P. Jacobsen, J. R. Thompson, and M. Christopher, “The changing automotive environment: high-temperature electronics,” *IEEE Trans. Electron. Packag. Manuf.*, vol. 27, no. 3, pp. 164–176, Jul. 2004, doi: 10.1109/TEPM.2004.843109.
- [5] Z. Galazka, “ β -Ga₂O₃ for wide-bandgap electronics and optoelectronics,” *Semicond. Sci. Technol.*, vol. 33, no. 11, p. 113001, 2018.
- [6] R. M. Kotecha *et al.*, “Electrothermal Modeling and Analysis of Gallium Oxide Power Switching Devices,” doi: 10.1115/IPACK2019-6453.
- [7] H. Huang *et al.*, “Robust Deep UV Photodetectors Based on One-Step-Grown Polycrystalline Ga₂O₃ Film via Pulsed Laser Deposition toward Extreme-Environment Application,” *Adv. Opt. Mater.*, vol. 12, no. 24, p. 2400788, 2024.
- [8] M. Baldini, Z. Galazka, and G. Wagner, “Recent progress in the growth of β -Ga₂O₃ for power electronics applications,” *Mater. Sci. Semicond. Process.*, vol. 78, pp. 132–146, 2018.
- [9] R. Sun, A. R. Balog, H. Yang, N. Alem, and M. A. Scarpulla, “Degradation of β -Ga₂O₃ vertical Ni/Au Schottky diodes under forward bias,” *IEEE Electron Device Lett.*, vol. 44, no. 5, pp. 725–728, 2023.
- [10] C. Hou, R. M. Gazoni, R. J. Reeves, and M. W. Allen, “High-Temperature β -Ga₂O₃ Schottky Diodes and UVC Photodetectors Using RuO_x Contacts,” *IEEE Electron Device Lett.*, vol. 40, no. 10, pp. 1587–1590, Oct. 2019, doi: 10.1109/LED.2019.2937494.
- [11] C. Fares, F. Ren, and S. J. Pearton, “Temperature-Dependent Electrical Characteristics of β -Ga₂O₃ Diodes with W Schottky Contacts up to 500°C,” *ECS J. Solid State Sci. Technol.*, vol. 8, no. 7, p. Q3007, Dec. 2018, doi: 10.1149/2.0011907jss.
- [12] W. Li, Y. Saraswat, K. Nomoto, D. Jena, and H. G. Xing, “Near-ideal reverse leakage current and practical maximum electric field in β -Ga₂O₃ Schottky barrier diodes,” *Appl. Phys. Lett.*, vol. 116, no. 19, 2020.
- [13] Y.-H. Hong *et al.*, “The optimized interface characteristics of β -Ga₂O₃ Schottky barrier diode with low temperature annealing,” *Appl. Phys. Lett.*, vol. 119, no. 13, 2021.
- [14] P. Dong *et al.*, “6 kV/3.4 mΩ·cm² Vertical β -Ga₂O₃ Schottky Barrier Diode With BV₂/Ron,sp Performance Exceeding 1-D Unipolar Limit of GaN and SiC,” *IEEE Electron Device Lett.*, vol. 43, no. 5, pp. 765–768, 2022.
- [15] H.-C. Kim, V. Janardhanam, S. Pokhrel, and C.-J. Choi, “Epilayer thickness effect on the electrical and breakdown characteristics of vertical β -Ga₂O₃ Schottky barrier diode,” *J. Cryst. Growth*, vol. 649, p. 127941, Jan. 2025, doi: 10.1016/j.jcrysgro.2024.127941.
- [16] I. Rahaman *et al.*, “Epitaxial Growth of Ga₂O₃: A Review,” *Materials*, vol. 17, no. 17, p. 4261, 2024.
- [17] T. Harada, S. Ito, and A. Tsukazaki, “Electric dipole effect in PdCoO₂/ β -Ga₂O₃ Schottky diodes for high-temperature operation,” *Sci. Adv.*, vol. 5, no. 10, p. 5733, 2019.
- [18] Z. A. Jian, S. Mohanty, and E. Ahmadi, “Temperature-dependent current-voltage characteristics of β -Ga₂O₃ trench Schottky barrier diodes,” *Appl. Phys. Lett.*, vol. 116, 2020.
- [19] B. Wang *et al.*, “High-voltage vertical Ga₂O₃ power rectifiers operational at high temperatures up to 600 K,” *Appl. Phys. Lett.*, vol. 115, no. 26, p. 263503, Dec. 2019, doi: 10.1063/1.5132818.
- [20] J.-S. Li, *et al.*, “Superior high temperature performance of 8 kV NiO/Ga₂O₃ vertical heterojunction rectifiers,” *J. Mater. Chem. C*, vol. 11, no. 23, pp. 7750–7757, 2023.
- [21] T.-H. Yang *et al.*, “Temperature-dependent electrical properties of β -Ga₂O₃ Schottky barrier diodes on highly doped single-crystal substrates,” *J. Semicond.*, vol. 40, no. 1, p. 012801, Jan. 2019, doi: 10.1088/1674-4926/40/1/012801.
- [22] Ş. Altındal, A. F. Özdemir, Ş. Aydoğan, and A. Türüt, “Discrepancies in barrier heights obtained from current–voltage (IV) and capacitance–voltage (CV) of Au/PNoMPhPPy/n-GaAs structures in wide range of temperature,” *J. Mater. Sci. Mater. Electron.*, vol. 33, no. 15, pp. 12210–12223, May 2022, doi: 10.1007/s10854-022-08181-1.
- [23] I. Ohdomari and K.-N. Tu, “Parallel silicide contacts,” *J. Appl. Phys.*, vol. 51, no. 7, pp. 3735–3739, 1980.
- [24] Y. Song, R. Van Meirhaeghe, W. Laflere, and F. Cardon, “On the difference in apparent barrier height as obtained from capacitance-voltage and current-voltage-temperature measurements on Al/p-InP Schottky barriers,” *Solid-State Electron.*, vol. 29, no. 6, pp. 633–638, 1986.
- [25] A. Ahaitouf, *et al.*, “Interface state effects in GaN Schottky diodes,” *Thin Solid Films*, vol. 522, pp. 345–351, 2012.
- [26] P. Chattopadhyay, “Capacitance technique for the determination of interface state density of metal-semiconductor contact,” *Solid-State Electron.*, vol. 39, no. 10, pp. 1491–1493, 1996.
- [27] S. Banerjee and W. A. Anderson, “Temperature dependence of shunt resistance in photovoltaic devices,” *Appl. Phys. Lett.*, vol. 49, no. 1, pp. 38–40, Jul. 1986, doi: 10.1063/1.97076.
- [28] S. Zhang *et al.*, “High Breakdown Electric Field Diamond Schottky Barrier Diode With SnO₂ Field Plate,” *IEEE Trans. Electron Devices*, vol. 69, no. 12, pp. 6917–6921, Dec. 2022, doi: 10.1109/TED.2022.3216534.
- [29] E. H. Roderick and R. H. Williams, *Metal-semiconductor contacts*, vol. 129. Clarendon press Oxford, 1988.
- [30] A. Jayawardena and S. Dhar, “Analysis of temperature dependent forward characteristics of Ni/ β -Ga₂O₃ Schottky diodes,” *Semicond. Sci. Technol.*, vol. 31, no. 11, p. 115002, 2016.
- [31] D. H. Lee, K. Nomura, T. Kamiya, and H. Hosono, “Diffusion-Limited a-IGZO/Pt Schottky Junction Fabricated at 200C on a Flexible Substrate,” *IEEE Electron Device Lett.*, vol. 32, no. 12, pp. 1695–1697, 2011.
- [32] J. H. Werner and H. H. Güttler, “Barrier inhomogeneities at Schottky contacts,” *J. Appl. Phys.*, vol. 69, no. 3, pp. 1522–1533, 1991.
- [33] G. Jian *et al.*, “Characterization of the inhomogeneous barrier distribution in a Pt/(100) β -Ga₂O₃ Schottky diode via its temperature-dependent electrical properties,” *AIP Adv.*, vol. 8, no. 1, 2018.
- [34] Y. Son and R. L. Peterson, “The effects of localized tail states on charge transport mechanisms in amorphous zinc tin

- oxide Schottky diodes,” *Semicond. Sci. Technol.*, vol. 32, no. 12, p. 12LT02, Nov. 2017, doi: 10.1088/1361-6641/aa95d2.
- [35] S. Chand and J. Kumar, “Effects of barrier height distribution on the behavior of a Schottky diode,” *J. Appl. Phys.*, vol. 82, no. 10, pp. 5005–5010, Nov. 1997, doi: 10.1063/1.366370.
- [36] J. Freeouf, T. Jackson, S. Laux, and J. Woodall, “Effective barrier heights of mixed phase contacts: Size effects,” *Appl. Phys. Lett.*, vol. 40, no. 7, pp. 634–636, 1982.
- [37] I. Ohdomari, T. Kuan, and K.-N. Tu, “Microstructure and Schottky barrier height of iridium silicides formed on silicon,” *J. Appl. Phys.*, vol. 50, no. 11, pp. 7020–7029, 1979.
- [38] S. Pandey and S. Kal, “A simple approach to the capacitance technique for determination of interface state density of a metal–semiconductor contact,” *Solid-State Electron.*, vol. 42, no. 6, pp. 943–949, 1998.
- [39] J. Wang *et al.*, “Fabrication of Dual-Barrier Planar Structure Diamond Schottky Diodes by Rapid Thermal Annealing,” *IEEE Trans. Electron Devices*, vol. 68, no. 3, pp. 1176–1180, 2021.
- [40] G. Güler, Ş. Karataş, Ö. Güllü, and Ö. F. Bakkaloğlu, “The analysis of lateral distribution of barrier height in identically prepared Co/n-Si Schottky diodes,” *J. Alloys Compd.*, vol. 486, no. 1–2, pp. 343–347, 2009.
- [41] K. Heinselman, P. Walker, A. Norman, P. Parilla, D. Ginley, and A. Zakutayev, “Performance and reliability of β -Ga₂O₃ Schottky barrier diodes at high temperature,” *J. Vac. Sci. Technol. A*, vol. 39, no. 4, 2021.
- [42] H. Iwano, S. Zaima, and Y. Yasuda, “Hopping conduction and localized states in p-Si wires formed by focused ion beam implantations,” *J. Vac. Sci. Technol. B Microelectron. Nanometer Struct. Process. Meas. Phenom.*, vol. 16, no. 4, pp. 2551–2554, 1998.
- [43] D. Yu, C. Wang, B. L. Wehrenberg, and P. Guyot-Sionnest, “Variable Range Hopping Conduction in Semiconductor Nanocrystal Solids,” *Phys. Rev. Lett.*, vol. 92, no. 21, p. 216802, 2004.
- [44] S. M. Sze, Y. Li, and K. K. Ng, *Physics of semiconductor devices*. John Wiley & sons, 2021.
- [45] C. Hou, R. M. Gazoni, R. J. Reeves, and M. W. Allen, “Oxidized Metal Schottky Contacts on (010) --Ga₂O₃,” *IEEE Electron Device Lett.*, vol. 40, no. 2, pp. 337–340, 2019.
- [46] C. Hou *et al.*, “High temperature (500 °C) operating limits of oxidized platinum group metal (PtOx, IrOx, PdOx, RuOx) Schottky contacts on β -Ga₂O₃,” *Appl. Phys. Lett.*, vol. 117, no. 20, 2020.
- [47] K. Egbo *et al.*, “NiGa₂O₄ interfacial layers in NiO/Ga₂O₃ heterojunction diodes at high temperature,” *Appl. Phys. Lett.*, vol. 124, no. 17, 2024.
- [48] W. Hao *et al.*, “Low defect density and small I–V curve hysteresis in NiO/ β -Ga₂O₃ pn diode with a high PFOM of 0.65 GW/cm²,” *Appl. Phys. Lett.*, vol. 118, no. 4, p. 043501, Jan. 2021, doi: 10.1063/5.0038349.
- [49] W. A. Callahan, K. Egbo, C.-W. Lee, D. Ginley, R. O’Hayre, and A. Zakutayev, “Reliable operation of Cr₂O₃:Mg/ β -Ga₂O₃ p–n heterojunction diodes at 600 °C,” *Appl. Phys. Lett.*, vol. 124, no. 15, 2024.